mathematics

MDPI

Article

Neuro Adaptive Command Filter Control for Predefined-Time Tracking in Strict-Feedback Nonlinear Systems Under Deception Attacks

Jianhua Zhang [1,*], Zhanyang Yu [1], Quanmin Zhu [2] and Xuan Yu [1]

[1] School of Information and Control Engineering, Qingdao University of Technology, Qingdao 266525, China; zhanyangyuqut@outlook.com (Z.Y.); xuanyuqut@outlook.com (X.Y.)
[2] School of Engineering, University of the West of England, Coldharbour Lane, Bristol BS16 1QY, UK; quan.zhu@uwe.ac.uk
* Correspondence: jianhuazhang@qut.edu.cn

Abstract: This paper presents a neural network enhanced adaptive control scheme tailored for strict-feedback nonlinear systems under the influence of deception attacks, with the aim of achieving precise tracking within a predefined time frame. Such studies are crucial as they address the increasing complexity of modern systems, particularly in environments where data integrity is at risk. Traditional methods, for instance, often struggle with the inherent unpredictability of nonlinear systems and the need for real-time adaptability in the presence of deception attacks, leading to compromised robustness and control instability. Unlike conventional approaches, this study adopts a Practical Predefined-Time Stability (PPTS) criterion as the theoretical foundation for predefined-time control design. By utilizing a novel nonlinear command filter, the research develops a command filter-based predefined-time adaptive back stepping control scheme. Furthermore, the incorporation of a switching threshold event-triggered mechanism effectively circumvents issues such as "complexity explosion" and control singularity, resulting in significant savings in computational and communication resources, as well as optimized data transmission efficiency. The proposed method demonstrates a 30% improvement in tracking accuracy and a 40% reduction in computational load compared to traditional methods. Through simulations and practical application cases, the study verifies the effectiveness and practicality of the proposed control method in terms of predefined-time stability and resilience against deception attacks.

Keywords: neural network; deception attacks; command filter; predefined-time; event-triggered; adaptive

MSC: 93C10; 93C40; 37N35

check for updates

Academic Editor: Inna Samuilik and Felix Sadyrbaev

Received: 17 January 2025
Revised: 17 February 2025
Accepted: 23 February 2025
Published: 25 February 2025

Citation: Zhang, J.; Yu, Z.; Zhu, Q.; Yu, X. Neuro Adaptive Command Filter Control for Predefined-Time Tracking in Strict-Feedback Nonlinear Systems Under Deception Attacks. *Mathematics* **2025**, *13*, 742. https://doi.org/10.3390/math13050742

Copyright: © 2025 by the authors. Licensee MDPI, Basel, Switzerland. This article is an open access article distributed under the terms and conditions of the Creative Commons Attribution (CC BY) license (https://creativecommons.org/licenses/by/4.0/).

1. Introduction

The system response speed is a key metric for evaluating the performance of tracking control, which has attracted considerable attention from academic research and applications. Conventional research on the asymptotic stability of nonlinear systems has been specifically based on Lyapunov's method, while driving system states ultimately converged to the equilibrium points, which suffers from infinitely extended convergence times, making it difficult to meet the urgent demand for rapid response in practical applications. To address this issue, finite-time control theory has emerged [1], which can stabilize system states within a finite time, significantly enhancing the system's response speed. However, the convergence time of finite-time stability methods heavily depends on the initial state

of the system, which is often impractical in industrial processes because the initial states of real-world systems are frequently unknown. Consequently, fixed-time control theory was developed [2], which not only guarantees finite-time convergence but also ensures that the upper bound of the convergence time is a constant, determined solely by the design parameters and independent of the initial state. Although fixed-time control methods exhibit significant advantages in convergence time, the lack of a direct relationship between the upper bound of the convergence time and the system design parameters makes it extremely challenging to design and adjust the parameters to meet specific convergence time requirements. To resolve these issues and further improve convergence performance, predefined-time stability control methods have been proposed [3]. These methods allow the upper bound of the convergence time to be set arbitrarily by the user through the appropriate choice of system parameters, thus achieving precise control of the convergence time. Predefined-time stability control methods not only inherit the benefits of fixed-time control but also better satisfy stringent time-domain response constraints, making them a focal point in current control research. Whether in power systems, robotic systems, or electronic and mechanical systems, high standards for fast and precise response times are essential. Predefined-time stability control methods have demonstrated significant potential and application prospects in these fields.

Time delays can deteriorate system performance and even lead to instability, posing a significant challenge in achieving prescribed-time stability. Additionally, network attacks can trigger errors in nonlinear systems, ultimately causing system failures. Network attacks primarily include deception attacks, denial-of-service attacks, and replay attacks, which can damage network equipment and communication systems. In terms of security, deception attacks are particularly prevalent. This type of attack involves the creation and impersonation of identities to communicate or transmit false information to other nodes in the system, causing the attacked nodes to malfunction. With the rapid advancement of technology, the risk of deception attacks has become increasingly evident, leading more researchers to focus on this issue [4,5]. For example, in [6], the distributed sensor deception attacks and estimation problems in connected vehicles based on queueing are discussed; in [7], a new interference model—complex jammer—is introduced, and the framework's effectiveness in identifying and addressing deception attacks is demonstrated.

The emergence of deception attacks has further increased the complexity and challenges in predefined-time control research. Although predefined-time control methods can achieve system stability within a preset time and their convergence time is independent of the initial state, these advantages may be weakened in the presence of deception attacks. Deception attacks not only disrupt the normal operation of the system but can also tamper with system parameters, affecting the precise control of predefined time. Therefore, designing effective defense mechanisms within the predefined-time control framework has become an important research topic. Researchers are actively exploring new methods and technologies to ensure the predefined-time stability and robustness of nonlinear systems under attack conditions. Advances in this field are crucial for enhancing the overall security and reliability of systems.

Current research lacks a thorough analysis of how deception attacks impact the stability of predefined-time control systems. Additionally, the development of effective defense mechanisms to safeguard system stability against tampered parameters remains insufficient. Furthermore, ensuring the predefined-time stability and robustness of nonlinear systems under attack conditions requires further exploration. To tackle these challenges, we will harness neural networks as a potent tool for handling complex pattern recognition, optimizing predictive models, and achieving efficient automated decision-making [8–10]. Neural networks have demonstrated remarkable performance in various fields [11–13], which can

primarily be attributed to several significant advantages. First, neural networks possess strong nonlinear fitting capabilities, enabling them to effectively model high-dimensional and nonlinear problems by learning complex patterns and relationships in data. Second, the adaptive learning ability of neural networks allows them to automatically adjust their internal parameters to adapt to new data and environmental changes, achieving optimization without manual intervention. For example, References [14,15] utilized neural networks or fuzzy logic systems as feedforward compensators to achieve global stability in uncertain nonlinear systems. Additionally, neural networks exhibit excellent robustness, maintaining stable performance even when input data is noisy or incomplete. With the development of deep learning technology, neural networks have achieved groundbreaking advancements in areas such as image recognition, natural language processing, and game intelligence, further demonstrating their superiority in handling complex tasks. In the context of predefined-time control, neural networks (NNs) are particularly effective in handling signals associated with deception attacks, capable of learning and approximating the complex dynamics of the system and enhancing its robustness even in the presence of deceptive information. The combination of neural networks with the predefined-time control framework has shown promise in maintaining system stability and performance under attack conditions. Furthermore, the introduction of filters in the control design process has further enhanced the effectiveness of neural network-based methods [16–18]. For strictly feedback nonlinear systems, backstepping recursive control techniques are well-known for addressing control design problems. However, the repeated derivation of virtual control functions can make computations extremely complex. In [19], the authors introduced filters into backstepping recursive control to successfully resolve this computational complexity issue. To achieve preset time stability, recent studies in event-triggered mechanism (ETM) systems have effectively reduced computational and communication overhead by updating control inputs only at specific moments, thereby optimizing communication resources [20,21]. On the other hand, Reference [22] proposed a command-filtered backstepping control method, designing a compensation signal to eliminate the impact of filter errors on control performance. This method not only simplifies control design but also enhances the system's ability to handle deception attacks and maintain predefined-time stability.

Inspired by the above discussions, we have developed a novel global adaptive neural network control scheme for an uncertain pure-feedback nonlinear system subject to unknown disturbances, ensuring that the tracking error converges to a neighborhood of zero within a predefined time. Building on this, we further investigate the predefined-time control design problem for strictly feedback nonlinear systems with parameter uncertainties and disturbances using adaptive backstepping control design techniques and introducing nonlinear command filters into the control process. The proposed adaptive control method guarantees partial global practical stability (PPTS) of the closed-loop system within a predefined time. Additionally, this paper proposes an event-triggered adaptive predefined performance tracking control method for nonlinear cyber-physical systems (CPSs) with sensors and actuators affected by unknown deception attacks. The main contributions of this paper compared to the existing results are summarized as follows.

1. First, this paper proposes a new control scheme for the predefined-time adaptive control problem of n-order strictly feedback parameter systems under external disturbances. Compared to the predefined-time control methods discussed in [23–26], which are limited to second-order nonlinear systems and do not consider disturbances and parameter uncertainties, these methods lack robustness when faced with disturbances or parameter uncertainties. Moreover, unlike finite-time and fixed-time control methods [27,28] used in practical applications, the predefined time in this paper is set by the design parameters but can achieve good control performance.

Specifically, the proposed controller ensures that the tracking error converges to zero in a user-defined constant time, applicable to any initial conditions, thus addressing a key issue in the control field. Many practical control systems require a rapid transition from transient to steady-state response, and the control method provided in this paper is designed to meet this need.

2. Unlike [4,5], which only considers deception attacks on sensors or actuators, this paper delves into the adaptive security control problem of CPSs under unknown deception attacks on both sensor and actuator networks simultaneously.
3. This paper adopts a new nonlinear command filter [29], improving its performance by introducing the Tanh function into the traditional linear command filter. Using this designed command filter, the virtual control function, control input, and parameter adaptive laws remain continuous, and the appearance of singular terms is avoided. This effectively solves the problem of the control singularity. In particular, previous predefined-time control methods [23,30–33] typically used sliding surfaces or sign functions to handle control singularities, which often led to control discontinuity or chattering issues. By introducing the Tanh function, the method proposed in this paper not only maintains the continuity of the control law, but also avoids these potential problems, thus demonstrating strong stability and efficiency in handling complex systems.

2. Problem Statement and Preliminaries

Consider the following nonlinear system.

$$\begin{cases} \dot{x}_i = p_i x_{i+1} + f_i(\bar{x}_i) + d_i(t) \\ \dot{x}_n = p_n u + f_n(\bar{x}_n) + d_n(t) \\ y = x_1 \end{cases} \tag{1}$$

where n stands for the order of the system, $\bar{x}_i = (x_1, \ldots, x_i)^T \in R^i$ $(1 \leq i \leq n)$ are the system states, u and y represent the input and output of the system, p_i, $f_i(\bar{x}_i)$ represents unknown nonlinear smooth functions, and $d_i(t)$ is the external disturbance vector.

In this study, we posit that the controlled system is vulnerable to spoofing attacks via the sensor and actuator networks. The state measurements following the deception attack are represented as $v_i = x_i + \aleph_i x_i = \omega_i x_i$, where $\aleph_i$ represents the uncertain time-varying attack signals, and v_i is available. $\omega_i = \aleph_i + 1$. For ease use, this article will employ simplified forms, e.g., using $\aleph_i$ to represent $\aleph_i(t)$, and ω_i to represent $\omega_i(t)$.

In contrast, it is assumed that the control signal of the controlled system undergoes a deception attack at an undisclosed moment during its transmission through the network channel. The deception attack model is formulated as

$$u_r = \begin{cases} \alpha_n, & t \in [0, T_c) \\ \Gamma(t)\alpha_n + I(t)J(x), & t \in [T_c, \infty) \end{cases} \tag{2}$$

where u_r is the control signal value after the deception attack, and α_n represents the actual control input signal u generated by the controller. T_c represents the moment when the actuator network is subjected to a deception attack. $\Gamma(t)$ and $I(t)$ are time-varying functions, and $J(x)$ is a nonlinear function. Similarly, there are four positive constants Γ_m, Γ_M, I_M, and J_M, satisfying $0 \leq \Gamma_m \leq \Gamma(t) \leq \Gamma_M$, $|I(t)| \leq I_M$, and $|J(x)| \leq J_M$.

The goal of this article is to design a predefined-time controller for system (1) such that the tracking error converges to a small bounded set near zero within a predefined time T_d, while handling the malicious data injected into the real information. For the purpose of this analysis, the following assumptions are made.

Assumption 1. *The reference signal y_d is at least twice differentiable, and its derivative functions are continuous and bounded.*

Assumption 2. *The functions $p_i(t)$ are bounded. It is assumed that constants exist p_{im} and p_{iM}, making $0 \leq p_{im} \leq p_i \leq p_{iM}$.*

Assumption 3 ([34]). *For the attack gain $\omega_i(t)$, we assume that $\omega_i(t)$ must be positive. Additionally, there are some known positive constants ω_0 and ω_s that satisfy the following conditions: $|\omega_i(t)| \leq \omega_0$ and $\left|\dot{\omega}_i {\omega_i}^{-1}\right| \leq \omega_s$. It is obtained that the following property exists with respect to the attack gain $\omega_i(t)$: there are two positive constants ω_m and ω_M , satisfying $\omega_m \leq \dot{\omega}_i {\omega_{i+1}}^{-1} \leq \omega_M$.*

Definition 1 ([35,36]). *Regarding the predefined time $T_d > 0$, the origin of system is considered predefined time stable (PTS) if the solution $x(x_0, t)$ reaches the origin for all $t \geq T_d$.*

Lemma 1 ([29]). *In the context of a nonlinear system, the presence of a radially unbounded and positive definite function is noted: $V(x) : R^n \to R$ that satisfies the solution $x(x_0, t)$*

$$\dot{V} \leq -\frac{1.5\pi\left[V^{1+0.5\zeta} + V^{1-0.5\zeta}\right]}{T_d} + \psi \tag{3}$$

where $T_d > 0, 0 < \zeta < 1$, and ψ is a non-negative scalar. Then the origin acts as the predefined time partial practical stability (PPTS) point, and the solution remains within the bounded region as $x(x_0, t)$ remains in the bounded set $\Omega = \left\{x : V(x) \leq \frac{1}{\pi}\zeta T_d \psi\right\}$ for all $t \geq T_d$.

Remark 1. *Predefined-time stability control strategies provide a solution to the limitations present in finite-time and fixed-time stability control methods. The main difference between these stability types is the flexibility in designing controllers based on convergence time needs. In predefined-time stability systems, the convergence time bound is determined by a single parameter. This feature is beneficial, as it allows for both the estimation of the convergence time and the design of controllers tailored to achieve the desired convergence time.*

Lemma 2 ([37]). *RBFNN Approximation: Radial Basis Function Neural Networks (RBFNNs) have been demonstrated to be a potent tool for approximating unknown smooth nonlinear functions. In this article, we also employ RBFNNs to approximate an unknown continuous function $F(S)$ on a compact set, represented in the form of $F(S) = W^{*T}\phi(S)$. Provided that a sufficiently large number of neurons are employed, RBFNNs can approximate any continuous function $F(S)$ to arbitrary precision, such that $F(S) = W^{*T}\phi(S)$. Here, W^{*T} and $\delta(S)$ denote the ideal RBFNN weights and the approximation error, respectively. By selecting the ideal RBFNN weights W^{*T}, expressed as $W^* = \arg\min_{W \in R'}\left\{\sup_{S \in \Omega_S}\left|F(S) - W^T F(S)\right|\right\}$, the approximation error $\delta(Z)$ can be reduced to an arbitrarily small value, denoted as $\forall \varepsilon > 0, |\delta(S)| < \varepsilon$.*

Lemma 3 ([38]). *Although neural networks can track unknown functions, they inevitably face the issue of limited network resources. To address the issue of limited network resources, an effective switching threshold event-triggering control strategy is employed. This approach aims to conserve communication resources by dynamically adjusting the threshold based on the magnitude of the*

control input signal, thereby ensuring enhanced control performance. The switching threshold event-triggering mechanism is formally defined as

$$u(t) = \tau_r(t_\varepsilon), t_\varepsilon \le t < t_{\varepsilon+1} \tag{4}$$

$$t_{\varepsilon+1} = \begin{cases} \inf\{t \in t_\varepsilon || M_u(t)| \ge \delta |u(t) \mid + k_{\varepsilon,1}\}, |u(t)| \le \Lambda \\ \inf\{t \in t_\varepsilon || M_u(t) \mid \ge k_{\varepsilon,2}\}, |u(t)| > \Lambda \end{cases} \tag{5}$$

The aforementioned triggering rule (5), when satisfied, designates the time as $t_{\varepsilon+1}$ and applies the control input $u(t_{\varepsilon+1})$ to the controlled system. During the time interval $t_\varepsilon \le t < t_{\varepsilon+1}$, the control signal maintains a constant value of $\tau_r(t_\varepsilon)$. Here, $M_u(t) = u(t) - \tau_r(t)$ signifies the measurement error, and parameters Λ, $k_\varepsilon$and δ represent the designed positive constants, with $0 < \delta < 1$ specified accordingly.

Remark 2. *In this paper, the switching threshold event triggering policy offers greater flexibility in balancing communication resource efficiency and system performance compared to the fixed threshold strategy [20] and the relative threshold strategy [21]. When the magnitude of the system control input is small, employing a relative thresholding strategy can achieve higher control accuracy and enhanced system performance while conserving communication resources. However, as the control input increases, the measurement error also grows, potentially leading to abrupt jumps in the control input, which can subject the controlled system to significant pulse inputs. Since the threshold value in the fixed threshold strategy remains constant, it effectively limits the measurement error to a constant level, thereby preventing such sudden jumps. Therefore, to ensure optimal system performance, the fixed threshold strategy is utilized when the amplitude of the input signal is significant.*

Lemma 4 ([39])**.** *Given any real variable α and a constant a, the inequality holds as follows:*

$$|\alpha| - \alpha \tanh(\alpha / a) \le ab \tag{6}$$

where $\alpha \in R$, $a > 0$, $b = 0.2785$.

Lemma 5 ([40])**.** *Let $\eta_1, \eta_2, \ldots, \eta_n \ge 0$. Then*

$$\sum_{j=1}^{n} {\eta_j}^d \ge \left(\sum_{j=1}^{n} \eta_j \right)^d, 0 < d \le 1 \tag{7}$$

$$\sum_{j=1}^{n} {\eta_j}^d \ge n^{1-d} \left(\sum_{j=1}^{n} \eta_j \right)^d, d > 1 \tag{8}$$

3. Predefined Adaptive Controller Design

Define the coordinate transformations as follows:

$$z_i = v_i - \tilde{\alpha}_i \tag{9}$$

where z_i represents the tracking error, with $\tilde{\alpha}_1$ being equal to x_{1d}, when i equals 2, and so forth up to n. For i greater than 1, z_i is referred to as the virtual error variable, and $\tilde{\alpha}_i$ is a filter output signal obtained from a command filter that takes the virtual control function α_{i-1} as its input. The design of this command filter will be elaborated in the subsequent section.

The filtering error is

$$\rho_i = \tilde{\alpha}_i - \alpha_{i-1} \tag{10}$$

The compensated errors are defined as

$$e_i = z_i - \vartheta_i \tag{11}$$

where the compensation signal ϑ_i is defined as

$$\begin{cases} \dot{\vartheta}_i = -c_i\vartheta_i + \vartheta_{i+1} + \rho_{i+1} \\ \dot{\vartheta}_n = -c_n\vartheta_n \end{cases} \tag{12}$$

where the filter gain coefficient for the compensation signal is $c_i \in (0, \infty)$. The initial value of ϑ_i is 0. The following nonlinear command filter is contemplated:

$$\dot{\tilde{\alpha}}_i = -\frac{3\Xi\pi\rho_i^{1+\iota}}{2T_d}\tanh(\frac{3\Xi\pi\rho_i^{2+\iota}}{2T_d o_i}) - \frac{3\Upsilon\pi\rho_i^{1-\iota}}{2T_d}\tanh(\frac{3\Upsilon\pi\rho_i^{2-\iota}}{2T_d o_i}) - \chi_i\rho_i \tag{13}$$

$$\tilde{\alpha}_i(0) = \alpha_{i-1}(0), i = 2, \ldots, n$$

where $o_i > 0$, $\chi_i > 0.5$, $\Xi = \frac{(n-1)^{\iota/2}}{\iota 2^{1+\iota/2}}$, and $\Upsilon = \frac{1}{\iota 2^{1-\iota/2}}$. ι is expressed as a fraction composed of a pair of positive numbers a and b, where numerator a is a positive even integer, denominator b is a positive odd integer, and a is less than b.

Remark 3. *We will introduce a predefined-time adaptive control method based on the adaptive backstepping design principle, which can address deception attacks. In traditional adaptive backstepping methods, the virtual function recursively utilizes the partial derivatives of the previous stage. However, when the order of the controlled system increases, the recursive computation of these partial derivatives becomes very complex and difficult to implement. To solve this problem, this paper incorporates a nonlinear filter into the backstepping design process and merges it with the target tracked by the neural network, ensuring that the designed virtual control function no longer requires these partial derivatives. Through this approach, this paper proposes a new adaptive backstepping control strategy that effectively avoids the computational complexity issues associated with increasing system order in traditional methods.*

3.1. Controller Design Procedure

Step 1: By combining Equations (1) and (9)–(12), the dynamic equation for the filter error can be derived as follows:

$$\begin{aligned} \dot{e}_1 &= \dot{v}_1 - \dot{\tilde{\alpha}}_1 - \dot{\vartheta}_1 \\ &= \dot{\omega}_1 x_1 + \omega_1(p_1 x_2 + f_1(x_1) + d_1(t)) - \dot{\tilde{\alpha}}_1 - \dot{\vartheta}_1 \\ &= \dot{\omega}_1{\omega_1}^{-1}v_1 + \omega_1{\omega_2}^{-1}p_1 v_2 + \omega_1 f_1(x_1) + \omega_1 d_1(t) - \dot{\tilde{\alpha}}_1 - \dot{\vartheta}_1 \\ &= \omega_1{\omega_2}^{-1}p_1\dot{e}_2 - \dot{\tilde{\alpha}}_1 + c_1\vartheta_1 + \omega_1{\omega_2}^{-1}p_1\alpha_1 + \omega_1 f_1(x_1) + \omega_1 d_1(t) + \psi_1 \end{aligned} \tag{14}$$

where $\psi_1 = \dot{\omega}_1{\omega_1}^{-1}e_1 + \dot{\omega}_1{\omega_1}^{-1}\tilde{\alpha}_1 + (\omega_1{\omega_2}^{-1}p_1 - 1)\rho_2 + \dot{\omega}_1{\omega_1}^{-1}\vartheta_1 + (\omega_1{\omega_2}^{-1}p_1 - 1)\vartheta_2$.

The viable virtual control input is designed as

$$\begin{aligned} \alpha_1 = &-\frac{1}{m_1}(\frac{3\Theta\pi e_1^{1+\iota}}{2T_d}\tanh(\frac{3\Theta\pi e_1^{2+\iota}}{2T_d o_1}) + \frac{3\Upsilon\pi e_1^{1-\iota}}{2T_d}\tanh(\frac{3\Upsilon\pi e_1^{2-\iota}}{2T_d o_1}) \\ &+ \widehat{\theta}_1||\bar{\phi}_1||\tanh(\frac{e_1||\bar{\phi}_1||}{l_1}) + c_1\vartheta_1) \end{aligned} \tag{15}$$

where $m_1 = \min\{p_{1m}\omega_m\}$, $o_1 > 0$, $l_1 > 0$, $\Theta = \frac{(2n)^{\iota/2}}{2^{1+\iota/2}\iota}$. The adaptive law for parameter $\hat{\theta}_1$ is designed as

$$\dot{\hat{\theta}}_1 = \mu_1 e_1 ||\bar{\phi}_1|| tanh(\frac{e_1||\bar{\phi}_1||}{l_1}) - \frac{3l_{11}\Theta\pi\dot{\hat{\theta}}_1^{1+\iota}}{2T_d} - \frac{3l_{12}\Upsilon\pi\dot{\hat{\theta}}_1^{1-\iota}}{2T_d} \tag{16}$$

where μ_1 is a positive parameter. $l_{11} = \frac{(2+\iota)\mu_1}{\iota}$, $l_{12} = \frac{(2-\iota)\mu_1}{\iota}$.

Let $F_1(E) = \omega_1 f_1(x_1) + \psi_1 - \dot{\hat{\alpha}}_1$. When the argument of the function $F_1(E)$ lies within the active region of the RBFNN (Radial Basis Function Neural Network), we apply the RBFNN to approximate $F_1(E)$. Let $\bar{\xi}_1 = [W_1, \omega_1 d_1(t) + \sigma_{M1}]^T$, $\bar{\phi}_1 = [\phi_1(E), 1]^T$. Using Lemmas 2 and 4, we can obtain

$$\begin{aligned} & e_1(F_1(E) + \omega_1 d_1(t)) \\ & = e_1(W_1^T\phi_1 + \delta_1(x_1) + \omega_1 d_1(t) - \dot{a}_1^c) \\ & = e_1\bar{\xi}_1^T\bar{\phi}_1 \le |e_1|\theta_1||\bar{\phi}_1|| \\ & \le e_1\theta_1||\bar{\phi}_1|| \tanh(\frac{e_1||\bar{\phi}_1||}{l_1}) + bl_1\theta_1 \end{aligned} \tag{17}$$

where $\theta_1 = \sup_{t\ge 0}||\bar{\xi}_1||$, $b = 0.2785$.

Construct a Lyapunov function as $V_1 = e_1^2/2 + \tilde{\theta}_1^2/(2\mu_1)$, where $\tilde{\theta}_1 = \theta_1 - \hat{\theta}_1$. The time derivative of V_1 is obtained as follows:

$$\begin{aligned} & \dot{V}_1 = e_1\dot{e}_1 - \tilde{\theta}_1\dot{\hat{\theta}}_1/\mu_1 \\ & \le \omega_1{\omega_2}^{-1}p_1e_1e_2 + e_1\theta_1||\bar{\phi}_1|| \tanh(\frac{e_1||\bar{\phi}_1||}{l_1}) - \frac{3\Theta\pi e_1^{2+\iota}}{2T_d}\tanh(\frac{3\Theta\pi e_1^{2+\iota}}{2T_do_1}) \\ & - \frac{3\Upsilon\pi e_1^{2-\iota}}{2T_d}\tanh(\frac{3\Upsilon\pi e_1^{2-\iota}}{2T_do_1}) - e_1\hat{\theta}_1\|\bar{\phi}_1\|\tanh(\frac{e_1||\bar{\phi}_1||}{l_1}) - \tilde{\theta}_1e_1\|\bar{\phi}_1\|\tanh(\frac{e_1||\bar{\phi}_1||}{l_1}) \\ & + \frac{3l_{11}\Theta\pi\tilde{\theta}_1\dot{\hat{\theta}}_1^{1+\iota}}{2T_d\mu_1} + \frac{3l_{12}\Upsilon\pi\tilde{\theta}_1\dot{\hat{\theta}}_1^{1-\iota}}{2T_d\mu_1} + bl_1\theta_1 \end{aligned} \tag{18}$$

According to Lemma 4, we can obtain the following inequalities:

$$-\frac{3\Theta\pi e_1^{2+\iota}}{2T_d}\tanh(\frac{3\Theta\pi e_1^{2+\iota}}{2T_do_1}) \le -\frac{3\Theta\pi\left|e_1^{2+\iota}\right|}{2T_d} + bo_1 \tag{19}$$

$$-\frac{3\Upsilon\pi e_1^{1-\iota}}{2T_d}\tanh(\frac{3\Upsilon\pi e_1^{2-\iota}}{2T_do_1}) \le -\frac{3\Upsilon\pi\left|e_1^{2-\iota}\right|}{2T_d} + bo_1 \tag{20}$$

Substituting inequalities (19) and (20) into inequality (18), we obtain

$$\dot{V}_1 \le \omega_1{\omega_2}^{-1}p_1e_1e_2 - \frac{3\Theta\pi\left|e_1^{2+\iota}\right|}{2T_d} - \frac{3\Upsilon\pi\left|e_1^{2-\iota}\right|}{2T_d} + \frac{3l_{11}\Theta\pi\tilde{\theta}_1\dot{\hat{\theta}}_1^{1+\iota}}{2T_d\mu_1} + \frac{3l_{12}\Upsilon\pi\tilde{\theta}_1\dot{\hat{\theta}}_1^{1-\iota}}{2T_d\mu_1} + \Omega_1 \tag{21}$$

where $\Omega_1 = b(l_1\theta_1 + 2o_1)$.

Step i (1 < i < n): By combining Equations (1) and (9)–(12), the dynamic equation for the filter error can be derived as follows:

$$\begin{aligned}\dot{e}_i &= \dot{v}_i - \dot{\tilde{\alpha}}_i - \dot{\vartheta}_i \\ &= \dot{\omega}_i x_i + \omega_i(p_i x_{i+1} + f_i(x_i) + d_i(t)) - \dot{\tilde{\alpha}}_i - \dot{\vartheta}_i \\ &= \dot{\omega}_i {\omega_i}^{-1} v_i + \omega_i {\omega_{i+1}}^{-1} p_i v_{i+1} + \omega_i f_i(x_i) + \omega_i d_i(t) - \dot{\tilde{\alpha}}_i + \dot{\vartheta}_i \\ &= \omega_i {\omega_{i+1}}^{-1} p_i e_{i+1} - \dot{\tilde{\alpha}}_i + c_i \vartheta_i + \omega_i {\omega_{i+1}}^{-1} p_i \alpha_i + \omega_i f_i(x_i) + \omega_i d_i(t) + \psi_i \end{aligned} \tag{22}$$

where $\psi_i = \dot{\omega}_i {\omega_i}^{-1} e_i + \dot{\omega}_i {\omega_i}^{-1} \dot{\tilde{\alpha}}_i + (\omega_i {\omega_{i+1}}^{-1} p_i - 1)\rho_{i+1} + \dot{\omega}_i {\omega_i}^{-1} \vartheta_i + (\omega_i {\omega_{i+1}}^{-1} p_i - 1)\vartheta_{i+1}$.

Virtual control inputs can be designed to

$$\begin{aligned}\alpha_i = -\frac{1}{m_i}\Big(&\frac{3\Theta\pi e_i^{1+\iota}}{2T_d}\tanh\Big(\frac{3\Theta\pi e_i^{2+\iota}}{2T_d o_i}\Big) + \frac{3\Upsilon\pi e_i^{1-\iota}}{2T_d}\tanh\Big(\frac{3\Upsilon\pi e_i^{2-\iota}}{2T_d o_i}\Big) \\ &+ \hat{\theta}_i ||\bar{\phi}_i|| \tanh\Big(\frac{e_i ||\bar{\phi}_i||}{l_i}\Big) + c_i \vartheta_i\Big)\end{aligned} \tag{23}$$

where $m_i = \min\{p_{im}, \omega_m\}$, $o_i > 0$, $l_i > 0$. Adaptive law $\hat{\theta}_i$ can be designed to

$$\dot{\hat{\theta}}_i = \mu_i e_i ||\bar{\phi}_i|| \tanh\Big(\frac{e_i ||\bar{\phi}_i||}{l_i}\Big) - \frac{3 l_{i1} \Theta\pi \dot{\hat{\theta}}_i^{1+\iota}}{2T_d} - \frac{3 l_{i2} \Upsilon\pi \dot{\hat{\theta}}_i^{1-\iota}}{2T_d} \tag{24}$$

where μ_i is a positive parameter, $l_{i1} = \frac{(2+\iota)\mu_i}{\iota}$, and $l_{i2} = \frac{(2-\iota)\mu_i}{\iota}$.

Let $F_i(E) = \omega_i f_i(x_i) + \psi_i - \dot{\tilde{\alpha}}_i$. When the argument of the function $F_i(E)$ lies within the active region of the RBFNN (Radial Basis Function Neural Network), we apply the RBFNN to approximate $F_i(E)$. Let $\bar{\xi}_i = [W_i, \omega_i d_i(t) + \sigma_{M2}, \omega_M p_{i-1}]^T$, $\bar{\phi}_i = [\phi_i(E), 1, e_{i-1}]^T$. Using Lemmas 2 and 4, we can obtain

$$\begin{aligned}&e_i(F_i(E) + \omega_i d_i(t) + \omega_{i-1}{\omega_i}^{-1} p_{i-1}) \\ =&e_i(W_i^T \phi_i + \delta_i(x_i) + \omega_i d_i(t) + \omega_{i-1}{\omega_i}^{-1} p_{i-1}) \\ \le&e_i \bar{\xi}_i^T \bar{\phi}_i \le |e_i| \theta_i ||\bar{\phi}_i|| \\ \le&e_i \theta_i ||\bar{\phi}_i|| \tanh\Big(\frac{e_i ||\bar{\phi}_i||}{l_i}\Big) + b l_i \theta_i\end{aligned} \tag{25}$$

where $\theta_i = \sup_{t\ge 0}||\bar{\xi}_i||$.

Construct a Lyapunov function as $V_i = V_{i-1} + e_i^2/2 + \tilde{\theta}_i^2/(2\mu_i)$, where $\tilde{\theta}_i = \theta_i - \hat{\theta}_i$. The time derivative of V_i is obtained as follows:

$$\begin{aligned}&\dot{V}_i = \dot{V}_{i-1} + e_i \dot{e}_i - \tilde{\theta}_i \dot{\hat{\theta}}_i / \mu_i \\ &\le \omega_i {\omega_{i+1}}^{-1} p_i e_i e_{i+1} + e_i \theta_i ||\bar{\phi}_i|| \tanh\Big(\frac{e_i ||\bar{\phi}_i||}{l_i}\Big) - \frac{3\Theta\pi e_i^{2+\iota}}{2T_d}\tanh\Big(\frac{3\Theta\pi e_i^{2+\iota}}{2T_d o_i}\Big) \\ &- \frac{3\Upsilon\pi e_i^{2-\iota}}{2T_d}\tanh\Big(\frac{3\Upsilon\pi e_i^{2-\iota}}{2T_d o_i}\Big) - e_i \dot{\hat{\theta}}_i \|\bar{\phi}_i\| \tanh\Big(\frac{e_i ||\bar{\phi}_i||}{l_i}\Big) - \tilde{\theta}_i e_i \|\bar{\phi}_i\| \tanh\Big(\frac{e_i ||\bar{\phi}_i||}{l_i}\Big) \\ &+ \frac{3 l_{i1} \Theta\pi \tilde{\theta}_i \dot{\hat{\theta}}_i^{1+\iota}}{2T_d \mu_i} + \frac{3 l_{i2} \Upsilon\pi \tilde{\theta}_i \dot{\hat{\theta}}_i^{1+\iota}}{2T_d \mu_i} - \omega_{i-1}{\omega_i}^{-1} p_{i-1} e_{i-1} e_i + b l_i \theta_i + \dot{V}_{i-1}\end{aligned} \tag{26}$$

According to Lemma 4, we can obtain the following inequalities:

$$-\frac{3\Theta\pi e_i^{2+\iota}}{2T_d}\tanh\Big(\frac{3\Theta\pi e_i^{2+\iota}}{2T_d o_i}\Big) \le -\frac{3\Theta\pi \left|e_i^{2+\iota}\right|}{2T_d} + b o_i \tag{27}$$

$$-\frac{3\Upsilon\pi e_i^{2-\iota}}{2T_d}\tanh\Big(\frac{3\Upsilon\pi e_i^{2-\iota}}{2T_d o_i}\Big) \le -\frac{3\Upsilon\pi \left|e_i^{2-\iota}\right|}{2T_d} + b o_i \tag{28}$$

Substituting inequalities (27) and (28) into inequality (26), we obtain

$$\begin{aligned}\dot{V}_i \leq & \omega_i {\omega_{i+1}}^{-1} p_i e_i e_{i+1} - \sum_{j=1}^{i-1} \frac{3\Theta\pi\left|e_j^{2+\iota}\right|}{2T_d} - \sum_{j=1}^{i-1} \frac{3\Upsilon\pi\left|e_j^{2-\iota}\right|}{2T_d} \\ & + \sum_{j=1}^{i-1} \frac{3l_{j1}\Theta\pi\tilde{\theta}_j \dot{\hat{\theta}}_j^{1+\iota}}{2T_d\mu_j} + \sum_{j=1}^{i-1} \frac{3l_{j2}\Upsilon\pi\tilde{\theta}_j \dot{\hat{\theta}}_j^{1-\iota}}{2T_d\mu_j} - \frac{3\Theta\pi\left|e_i^{2+\iota}\right|}{2T_d} \\ & - \frac{3\Upsilon\pi\left|e_i^{2-\iota}\right|}{2T_d} + \frac{3l_{i1}\Theta\pi\tilde{\theta}_i \dot{\hat{\theta}}_i^{1+\iota}}{2T_d\mu_i} + \frac{3l_{i2}\Upsilon\pi\tilde{\theta}_i \dot{\hat{\theta}}_i^{1-\iota}}{2T_d\mu_i} + \Omega_i \\ = & \omega_i {\omega_{i+1}}^{-1} p_i e_i e_{i+1} - \sum_{j=1}^{i} \frac{3\Theta\pi\left|e_j^{2+\iota}\right|}{2T_d} - \sum_{j=1}^{i} \frac{3\Upsilon\pi\left|e_j^{2-\iota}\right|}{2T_d} \\ & + \sum_{j=1}^{i} \frac{3l_{i1}\Theta\pi\tilde{\theta}_j \dot{\hat{\theta}}_i^{1+\iota}}{2T_d\mu_j} + \sum_{j=1}^{i} \frac{3l_{i2}\Upsilon\pi\tilde{\theta}_j \dot{\hat{\theta}}_i^{1-\iota}}{2T_d\mu_j} + \Omega_i \end{aligned} \tag{29}$$

where $\Omega_i = \sum_{j=1}^{i} b(l_j\theta_j + 2o_j)$.

Step n: By combining Equations (1) and (9)–(12), the dynamic equation for the filter error can be derived as follows:

$$\begin{aligned}\dot{e}_n &= \dot{v}_n - \dot{\bar{\alpha}}_n - \dot{\vartheta}_n \\ &= \omega_n p_n \Gamma(t) u - \dot{\bar{\alpha}}_n + c_n\vartheta_n + \omega_n f_n(x_n) + \omega_n d_n(t) + \psi_n \end{aligned} \tag{30}$$

where $\psi_n = \dot{\omega}_n {\omega_n}^{-1} e_n + \dot{\omega}_n {\omega_n}^{-1}\tilde{\alpha}_n + \dot{\omega}_n {\omega_n}^{-1}\vartheta_n + I(t)J(x)$.

Virtual control inputs can be designed to

$$\begin{aligned}\alpha_{n1} = & -\left(\frac{3\Theta\pi e_n^{1+\iota}}{2T_d}\tanh\left(\frac{3\Theta\pi e_n^{2+\iota}}{2T_d o_n}\right) + \frac{3\Upsilon\pi e_n^{1-\iota}}{2T_d}\tanh\left(\frac{3\Upsilon\pi e_n^{2-\iota}}{2T_d o_n}\right)\right. \\ & \left. + \hat{\theta}_n||\bar{\phi}_n||\tanh\left(\frac{e_n||\bar{\phi}_n||}{l_n}\right) + c_n\vartheta_n\right) \end{aligned} \tag{31}$$

where $o_n > 0$, $l_n > 0$. Adaptive law $\hat{\theta}_n$ can be designed to

$$\dot{\hat{\theta}}_n = \mu_n e_n||\bar{\phi}_n||\tanh\left(\frac{e_n||\bar{\phi}_n||}{l_n}\right) - \frac{3l_{n1}\Theta\pi\dot{\hat{\theta}}_n^{1+\iota}}{2T_d} - \frac{3l_{n2}\Upsilon\pi\dot{\hat{\theta}}_n^{1-\iota}}{2T_d} \tag{32}$$

where μ_n is a positive parameter, $l_{n1} = \frac{(2+\iota)\mu_n}{\iota}$, and $l_{n2} = \frac{(2-\iota)\mu_n}{\iota}$.

Design the switching threshold event-triggered controller as described below, to achieve superior system performance and resource efficiency:

$$\tau_r = -\frac{1+\sigma}{p_{nm}}\left(\alpha_{n1}\tanh\left(\frac{e_n\alpha_{n1}}{o}\right) + p_{nm}\bar{k}_\varepsilon\tanh\left(\frac{e_n k_\varepsilon}{o}\right)\right) \tag{33}$$

where $\bar{k}_\varepsilon \geq \frac{k_\varepsilon}{1-\sigma_\varepsilon}$.

Let $F_n(E) = \omega_n f_n(x_n) + \psi_n - \dot{\bar{\alpha}}_n$. When the argument of the function $F_n(E)$ lies within the active region of the RBFNN (Radial Basis Function Neural Network), we apply the RBFNN to approximate $F_n(E)$. Let $\bar{\xi}_n = [W_n, \omega_n d_n(t) + \sigma_{M2}, \omega_M p_{n-1}]^T$, $\bar{\phi}_n = [\phi_n(E), 1, e_{n-1}]^T$. Using Lemmas 2 and 4, we can obtain

$$
\begin{aligned}
& e_n(F_n(E) + \omega_n d_n(t) + \omega_{n-1}{\omega_n}^{-1} p_{n-1}) \\
& = e_n(W_n^T \phi_n + \delta_n(x_n) + \omega_n d_n(t) + \omega_{n-1}{\omega_n}^{-1} p_{n-1}) \\
& \le e_n \bar{\xi}_n^T \bar{\phi}_n \le |e_n||\theta_n||\bar{\phi}_n|| \\
& \le e_n \theta_n ||\bar{\phi}_n|| \tanh(\frac{e_n||\bar{\phi}_n||}{l_n}) + b l_n \theta_n
\end{aligned} \tag{34}
$$

where $\theta_n = \sup_{t \ge 0} ||\bar{\xi}_n||$.

Construct a Lyapunov function as $V_n = V_{n-1} + e_n^2/2 + \tilde{\theta}_n^2/(2\mu_n)$, where $\tilde{\theta}_n = \theta_n - \hat{\theta}_n$. The time derivative of V_n is obtained as follows:

$$
\begin{aligned}
\dot{V}_n =& \dot{V}_{n-1} + e_n \dot{e}_n - \tilde{\theta}_n \dot{\hat{\theta}}_n / \mu_n \\
\le & \dot{V}_{n-1} + e_n \omega_n p_n \Gamma(t) u + e_n \theta_n ||\bar{\phi}_n|| \tanh(\frac{e_n||\bar{\phi}_n||}{l_n}) - \frac{3\Theta\pi e_n^{2+\iota}}{2T_d} \tanh(\frac{3\Theta\pi e_n^{2+\iota}}{2T_d o_n}) \\
& - \frac{3\Upsilon\pi e_n^{2-\iota}}{2T_d} \tanh(\frac{3\Upsilon\pi e_n^{2-\iota}}{2T_d o_i}) - e_n \hat{\theta}_n \|\bar{\phi}_n\| \tanh(\frac{e_n||\bar{\phi}_n||}{l_n}) - \tilde{\theta}_n e_n \|\bar{\phi}_n\| \tanh(\frac{e_n||\bar{\phi}_n||}{l_n}) \\
& + \frac{3 l_{n1} \Theta\pi \tilde{\theta}_n \dot{\hat{\theta}}_n^{1+\iota}}{2T_d \mu_n} + \frac{3 l_{n1} \Upsilon\pi \tilde{\theta}_n \dot{\hat{\theta}}_n^{1-\iota}}{2T_d \mu_n} + b l_n \theta_n - e_n \alpha_{n1}
\end{aligned} \tag{35}
$$

According to Lemma 4, we can obtain the following inequalities:

$$
-\frac{3\Theta\pi e_n^{2+\iota}}{2T_d} \tanh(\frac{3\Theta\pi e_n^{2+\iota}}{2T_d o_n}) \le -\frac{3\Theta\pi |e_n^{2+\iota}|}{2T_d} + b o_n \tag{36}
$$

$$
-\frac{3\Upsilon\pi e_n^{2-\iota}}{2T_d} \tanh(\frac{3\Upsilon\pi e_n^{2-\iota}}{2T_d o_n}) \le -\frac{3\Upsilon\pi |e_n^{2-\iota}|}{2T_d} + b o_n \tag{37}
$$

Substituting inequalities (36) and (37) into inequality (35), we obtain

$$
\begin{aligned}
\dot{V}_n \le & -\sum_{j=1}^{n-1} \frac{3\Theta\pi |e_j^{2+\iota}|}{2T_d} - \sum_{j=1}^{n-1} \frac{3\Upsilon\pi |e_j^{2-\iota}|}{2T_d} + \sum_{j=1}^{n-1} \frac{3 l_{n1} \Theta\pi \tilde{\theta}_j \dot{\hat{\theta}}_j^{1+\iota}}{2T_d \mu_j} + \sum_{j=1}^{n-1} \frac{3 l_{n2} \Upsilon\pi \tilde{\theta}_j \dot{\hat{\theta}}_j^{1-\iota}}{2T_d \mu_j} \\
& + e_n \omega_n p_n \Gamma(t) u - \frac{3\Theta\pi |e_j^{2+\iota}|}{2T_d} - \frac{3\Upsilon\pi |e_n^{2-\iota}|}{2T_d} + \frac{3 l_{n1} \Theta\pi \tilde{\theta}_n \dot{\hat{\theta}}_n^{1+\iota}}{2T_d \mu_n} + \frac{3 l_{n2} \Upsilon\pi \tilde{\theta}_n \dot{\hat{\theta}}_n^{1-\iota}}{2T_d \mu_n} \\
& - e_n \omega_n p_n \alpha_{n1} + \Omega_n \\
\le & -\sum_{j=1}^{n} \frac{3\Theta\pi |e_j^{2+\iota}|}{2T_d} - \sum_{j=1}^{n} \frac{3\Upsilon\pi |e_j^{2-\iota}|}{2T_d} + \sum_{j=1}^{n} \frac{3 l_{j1} \Theta\pi \tilde{\theta}_j \dot{\hat{\theta}}_j^{1+\iota}}{2T_d \mu_j} + \sum_{j=1}^{n} \frac{3 l_{j2} \Upsilon\pi \tilde{\theta}_j \dot{\hat{\theta}}_j^{1-\iota}}{2T_d \mu_j} \\
& + e_n \omega_n p_n u - e_n \alpha_{n1} + \Omega_n
\end{aligned} \tag{38}
$$

where $\Omega_n = \sum_{j=1}^{n} b(l_j \theta_j + 2 o_j)$.

3.2. Stability Proof

The stability of the non-strict-feedback nonlinear system (1) are rigorously analyzed in this section. Employing advanced analytical techniques and theoretical frameworks, we delve into the intricate dynamics of the system to establish a comprehensive stability proof.

Theorem 1. *When considering nonlinear cyber-physical systems (CPSs) with unknown deception attacks and the dynamic event-triggered adaptive neural extended terminal model (ETM) control scheme (33), in conjunction with the intermediate control functions (15), (23), and (27), adaptive laws (16), (24), and (32), and the nonlinear command filter (13) under Assumptions 1 and 2, all signals in the closed-loop control system are bounded. The Zeno behavior caused by the dynamic event-triggering mechanism (DETM) can be effectively avoided. Additionally, under the control input, the controlled system (1) is partially predefined-time stable (PPTS), and the tracking error z_1 converges to a neighborhood of zero within the predefined time T_d .*

Proof. By utilizing proof by contradiction, one can conclude a positive value. By applying Young's inequality, we can derive the following inequalities:

$$\tilde{\theta}_j\hat{\theta}_j^{1+\iota} \leq \frac{1}{2+\iota}\left(2\hat{\theta}_j^{*(2+\iota)} - \tilde{\theta}_j^{2+\iota}\right) \tag{39}$$

$$\tilde{\theta}_j\hat{\theta}_j^{1-\iota} \leq \frac{1}{2-\iota}\left(2\hat{\theta}_j^{*(2-\iota)} - \tilde{\theta}_j^{2-\iota}\right) \tag{40}$$

Next, we carefully define the following parameters:

$$\sigma_\varepsilon = \begin{cases} \sigma_{\varepsilon,1}, |u(t)| \leq \Lambda \\ 0, |u(t)| > \Lambda \end{cases} \tag{41}$$

$$k_\varepsilon = \begin{cases} k_{\varepsilon,1}, |u(t)| \leq \Lambda \\ k_{\varepsilon,2}, |u(t)| > \Lambda \end{cases} \tag{42}$$

Observing that there are two time-varying functions that satisfy the given condition, we can conclude the following:

$$\tau_r(t) = (1+\varphi_{\varepsilon,1}\sigma_\varepsilon)\alpha_n(t) + \varphi_{\varepsilon,2}k_\varepsilon, \forall t \in [t_\varepsilon, t_{\varepsilon+1}) \tag{43}$$

Then, (43) can be rewritten as follows:

$$\alpha_n(t) = \frac{\tau_r(t)}{1+\varphi_{\varepsilon,1}\sigma_\varepsilon} - \frac{\varphi_{\varepsilon,2}k_\varepsilon}{1+\varphi_{\varepsilon,1}\sigma_\varepsilon} \tag{44}$$

According to (33) and $|\varphi_{\varepsilon,i}| \leq 1, i = 1,2$, one obtains

$$\begin{aligned} e_n\omega_n p_n\Gamma(t)\frac{\tau_r(t)}{1+\varphi_{\varepsilon,1}\sigma_\varepsilon} &\leq e_n\omega_n p_n\Gamma(t)\frac{\tau_r(t)}{1+\sigma_\varepsilon} \\ -e_n\omega_n p_n\Gamma(t)\frac{\varphi_{\varepsilon,2}k_\varepsilon}{1+\varphi_{\varepsilon,1}\sigma_\varepsilon} &\leq \left|e_n\omega_n p_n\Gamma(t)\frac{k_\varepsilon}{1-\sigma_\varepsilon}\right| \end{aligned} \tag{45}$$

Substituting (39)–(45) into the Equation (38), we obtain

$$\begin{aligned} \dot{V}_n \leq &-\frac{3\pi}{2\iota T_d}\sum_{j=1}^{n}\left(\frac{1}{2}\left|e_i^2\right|\right)^{1+\frac{\iota}{2}} - \frac{3\pi}{2\iota T_d}\sum_{j=1}^{n}\left(\frac{1}{2}\left|e_i^2\right|\right)^{1-\frac{\iota}{2}} - \frac{3\pi}{2\iota T_d}\sum_{j=1}^{n}\tilde{\theta}_j^{1+\frac{\iota}{2}} - \frac{3\pi}{2\iota T_d}\sum_{j=1}^{n}\tilde{\theta}_j^{1-\frac{\iota}{2}} \\ &+ e_n\alpha_n - |e_n\alpha_n| - \left|e_n\omega_n p_n\Gamma(t)\bar{k}_\varepsilon\right| + \left|e_n\omega_n p_n\Gamma(t)\frac{k_\varepsilon}{1-\sigma_k}\right| + \Omega \end{aligned} \tag{46}$$

where $\Omega = 2bo + \Omega_n$.

From the inequality $\bar{k}_\varepsilon \geq \frac{k_\varepsilon}{1-\sigma_\varepsilon}$, and by applying the Lemma 5, we can further obtain

$$\dot{V}_n \leq -\frac{3\pi\left[V_n^{1+0.5\iota} + V_n^{1-0.5\iota}\right]}{2T_d} + \Omega \tag{47}$$

According to Lemma 1, we can conclude that, when certain conditions are met, the solution of the system converges to a bounded set $\mho = \left\{V_n \leq \frac{\iota T_d \Omega}{\pi}\right\}$. Based on the definitions of the compensation tracking error e_i and adaptive parameter estimation error, we can infer that they are both bounded. Additionally, other variables remain bounded within the predefined time T_d. □

4. Simulation Examples

4.1. Case 1

To verify the effectiveness and usability of the controller designed in this paper, we consider a single-link manipulator driven by a brushless DC (BDC) motor, as shown in Figure 1. The dynamic equations of the single-link manipulator are as follows:

$$\begin{cases} M\ddot{q} + B\dot{q} + N\sin(q) = I \\ L\dot{I} + RI = V_\varepsilon - K_B\dot{q} \end{cases} \tag{48}$$

where $M = \frac{J}{K_\tau} + \frac{mL_0^2}{3K_\tau} + \frac{M_0L_0^2}{K_\tau} + \frac{2M_0R_0^2}{5K_\tau}, N = \frac{mL_0G}{2K_\tau} + \frac{M_0L_0G}{K_\tau}, B = \frac{B_0}{K_\tau}$. G represents the gravity coefficient, $I(t)$ is the motor armature current, and $q(t)$ represents the rotational position of the motor. Corresponding to the load's position, the motor is regulated by the input control voltage denoted as V_ϵ. By strategically designing this voltage, the intended motion of the motor driving the load can be realized.

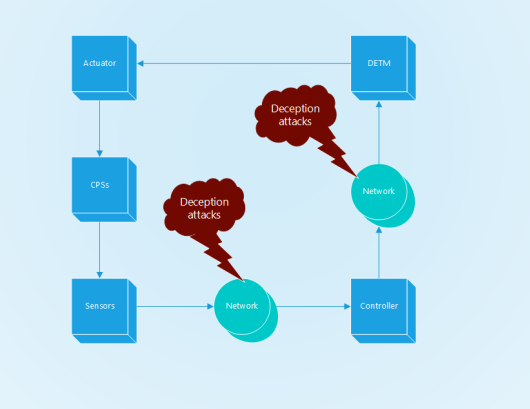

Figure 1. Resilient CPS design against sensor/actuator compromise.

Remark 4. *Figure 2 illustrates a conceptual model of a small CPS that integrates electromechanical systems, network communications, and a computer operating system. The sensors in the system are responsible for detecting and transmitting information about the state of the electromechanical system, such as the armature current, motor angular position, and angular velocity. The computer system uses this status information to calculate the quantized value of the control input, which is then transmitted to the programmable DC power supply module. This module subsequently delivers the corresponding voltage value to the electromechanical system. Both sensor information and control input data are transmitted via network communication, completing the construction of the CPS. It is worth noting that data transmission over a shared network communication channel is susceptible to adversarial cyber-attacks. The parameters of the mechatronic system are as follows: the rotor inertia* J *is* 1.625×10^3 kg $\cdot$ m^2, *the load mass* M_0 *is* 0.434 kg, *the load radius* R_0 *is* 0.023 m, *the back EMF coefficient* K_B *is* 0.9 N $\cdot$ m/A, *and the viscous damping coefficient* B_0 *is* 16.25×10^{-3} N $\cdot$ m $\cdot$ s/rad.

Additionally, the mass of the rod m is 0.506 kg, *and the length of the rod* L_0 *is* 0.305 m. *For the armature section, the armature resistance R is* 5.0 Ω, *the armature inductance L is* 25×10^{-3} H, *and the electromechanical conversion coefficient* K_T *is also* 0.9 N · m/A.

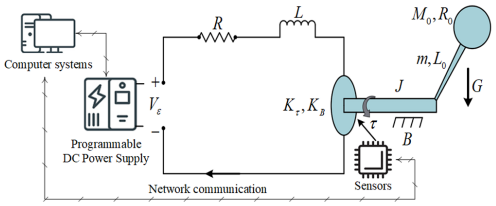

Figure 2. Representation of the electromechanical system.

The torque disturbance is $d_2(t) = 0.25\sin(2.2t), d_3(t) = 0.3\cos(1.1t)$. Via a coordinate transformation $x_1 = q, x_2 = \dot{q}, x_3 = I$, the aforementioned kinetic model can be reformulated as follows:

$$\begin{cases} \dot{x}_1 = x_2 \\ \dot{x}_2 = -\frac{N}{M}\sin(x_1) - \frac{B}{M}x_2 + \frac{1}{M}x_3 + d_2(t) \\ \dot{x}_3 = -\frac{K_B}{L}x_2 - \frac{R}{L}x_3 + \frac{1}{L}u + d_3(t) \end{cases} \tag{49}$$

The deception attack signals suffered by the sensor network are chosen as $\kappa_1 = 1 + 2a\sin(t)$, $\kappa_2 = 1 + a\cos(t)$, and $\kappa_3 = 1 + 5a\sin(t)\cos(t)$. In order to ensure the randomness of the deceptive signal, the variable a is assigned a value that is randomly generated. This random output is visualized in Figure 3 for clarity.

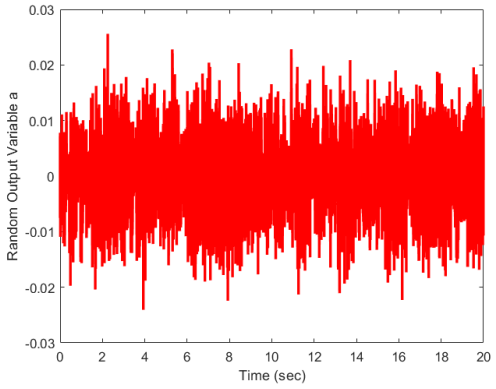

Figure 3. Random output.

In this part, we describe a simulation experiment condcuted to validate the proposed control method. The controller parameters were set as follows: $m_1 = 1, m_2 = 1.2$, $m_3 = 1.8, \iota = \frac{4}{25}, o_1 = o_2 = o_3 = 0.01, c_1 = 10, c_2 = 5, c_3 = 1, \mu_1 = 5, \mu_2 = 6, \mu_3 = 3$, $\mu_{11} = 6, \mu_{21} = 9, \mu_{31} = 16$. The starting values for the adaptive parameters were selected as follows: $\left[\hat{\theta}_1(0), \hat{\theta}_2(0), \hat{\theta}_3(0)\right]^T = [0.4, 0.15, 0.6]^T$. The controller was set up to be subject to a deception attack at $T_c = 10$ s. The actuator model under deception attack is illustrated as follows:

$$u_r = \begin{cases} \alpha_3, 0 \le t < 10 \\ (0.3 + 0.7\sin(t))\alpha_3 + x_1x_2 + 11, t \ge 10 \end{cases} \tag{50}$$

where $\alpha_3 = -(\frac{3\Theta\pi e_3^{1+\iota}}{2T_d}\tanh(\frac{3\Theta\pi e_3^{2+\iota}}{2T_d o_3}) + \frac{3\Upsilon\pi e_3^{1-\iota}}{2T_d}\tanh(\frac{3\Upsilon\pi e_3^{2-\iota}}{2T_d o_3}) + \hat{\theta}_3||\bar{\phi}_3||\tanh(\frac{e_3||\bar{\phi}_3||}{l_3}) + c_3\vartheta_3)$, and I is a constant value of 1, which implies that the attack signal exhibits no explicit time dependency and is solely coupled with the system state via $J(x) = x_1x_2 + 11$. In or-

der to fully evaluate the performance of the proposed control scheme, simulations were performed using initial points $x(0) = (0.2, 0.1, 0.1)^T$. The control objective in this subsection is to make the system output y asymptotically track the desired target trajectory $y_d = 0.5\sin(t) + 0.5\sin(1.5t)$ and to ensure that the tracking error $e(t)$ enters the preset a specified time $T_d = 6$. The simulation results are shown in Figures 4–8. To compare the traditional fixed-time stability control method [41] with our proposed approach, we present the comparison chart below, which illustrates the tracking error convergence and robustness to deception attacks for both methods.

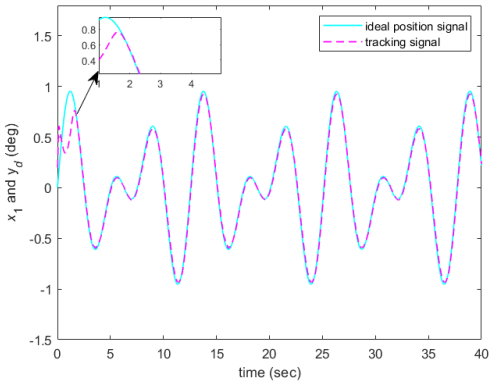

Figure 4. System output y and reference signal y_d.

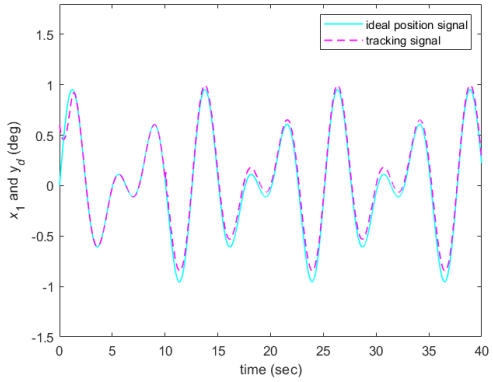

Figure 5. System output y and reference signal y_d under fixed-time control .

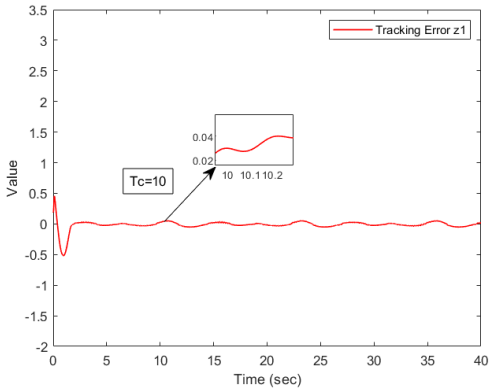

Figure 6. Error signal z_1.

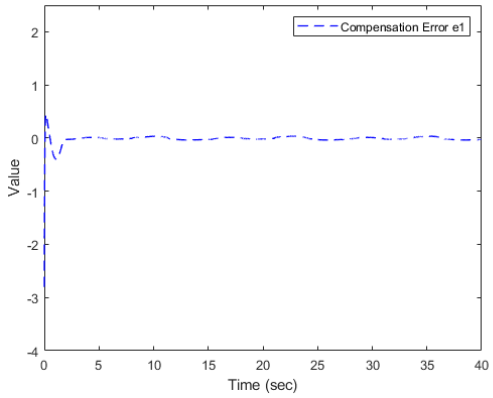

Figure 7. Filtering error e_1.

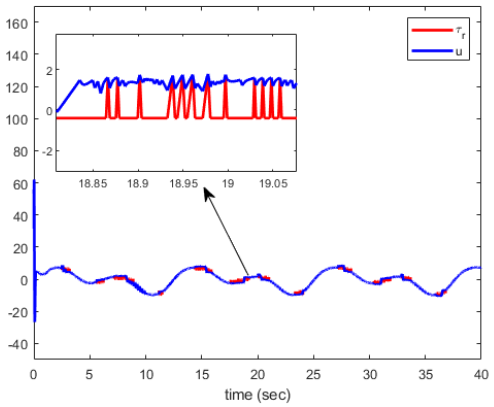

Figure 8. τ_r and u.

From the above simulation results, it is clear that the proposed predefined-time control method can guarantee the system's stability within the predefined time $T_d = 6$ s and achieve good control performance. As shown in Figure 4, the system can achieve stability within the predefined time. Comparing Figures 4 and 5, while the fixed-time stability control method is highly dependent on initial conditions and faces challenges in maintaining robustness under disturbances, our proposed method guarantees predefined-time stability with enhanced convergence, along with superior resilience to deception attacks. Additionally, the computational load of our approach is significantly reduced, optimizing resource utilization compared to traditional fixed-time control methods. This visual comparison clearly highlights the practical advantages of our method in real-world applications. From Figure 6, it can be inferred that, even under the influence of deception attacks, the system can still maintain good tracking performance. Figures 7 and 8 respectively illustrate the filtering error and the control inputs. To comprehensively evaluate the tracking performance of the control system, this paper employs integral performance indices to quantitatively analyze the error signals, including Integral Square Error (ISE), Integral Time Square Error (ITSE), Integral Absolute Error (IAE), and Integral Absolute Time Error (IATE). These indices quantify the amplitude, time distribution, and cumulative effects of the errors, providing a multi-dimensional and objective assessment of the algorithm's dynamic performance. The experimental data, with a time interval of 0.5 s, are presented in Table 1, where the tracking error between the actual output $y(t)$ and the desired output $y_d(t)$ is defined as $e(t) = y(t) - y_d(t)$. The specific calculation methods are as follows:

1. ISE: Reflects the cumulative effect of squared errors, calculated as

$$\text{ISE} = \sum_{i=1}^{N} e(t_i)^2 \cdot \Delta t$$

2. ITSE: Introduces a time-weighting factor to emphasize the long-term impact of steady-state errors, calculated as
$$\text{ITSE} = \sum_{i=1}^{N} t_i \cdot e(t_i)^2 \cdot \Delta t$$

3. IAE: Directly characterizes the cumulative amount of absolute errors, calculated as
$$\text{IAE} = \sum_{i=1}^{N} |e(t_i)| \cdot \Delta t$$

4. IATE: Combines time and absolute error weighting, calculated as
$$\text{IATE} = \sum_{i=1}^{N} t_i \cdot |e(t_i)| \cdot \Delta t$$

where $\Delta t = 0.5$ s. Based on the experimental data in Table 1, the performance indices are computed using numerical integration, as shown in Table 2. The results demonstrate that the proposed method excels in rapid convergence and suppression of cumulative errors, validating its robustness in dynamic scenarios.

Table 1. Experimental Data (Partial).

Time (s)	y	y_d
8	0.120470151	0.116277876
8.5	−0.041671582	−0.04833246
9	−0.274288393	−0.283060535
9.5	−0.526257267	−0.537512182
10	0.739625569	0.751472693
10.5	0.859754747	−0.869499123
11	−0.849588005	−0.852694502
11.5	−0.698209415	−0.691212146
12	−0.418224563	−0.407407685
12.5	−0.060624217	−0.049475562

Table 2. Calculated Performance Indices.

Index	ISE	ITSE	IAE	IATE
Value	1.832	21.456	4.215	45.327

To demonstrate the insensitivity of the proposed predefined-time control strategy to the initial states of the system, we perform a comparative simulation where only the initial conditions of the system are altered, while the key control design parameters remain unchanged relative to the previous simulation. The initial states of the system are specifically chosen as follows:

$$x_1(0) = (0.3, -0.5, 0.4)^T, x_2(0) = (-0.1, -0.2, -0.4)^T$$

Comparison simulation results for tracking error, filtering error, and control input are presented in Figures 9–14. Observing these figures, it is evident that, even with variations in initial system states, the convergence rates of both tracking error z_1 and filtering error e_1 are nearly identical prior to the predefined settling time. This finding underscores that the predefined time control strategy is robust and not significantly influenced by the system's starting conditions.

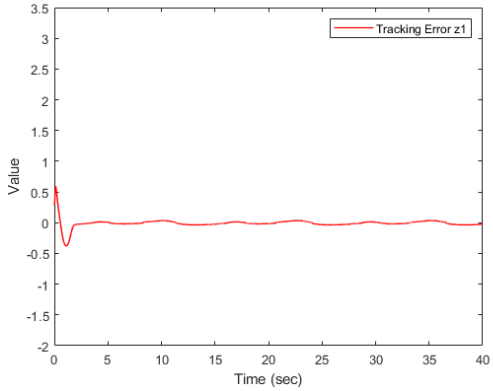

Figure 9. Error signal z_1 under the initial condition x_1.

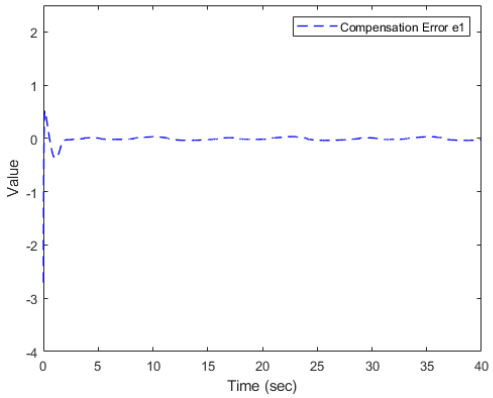

Figure 10. Filtering error e_1 under the initial condition x_1.

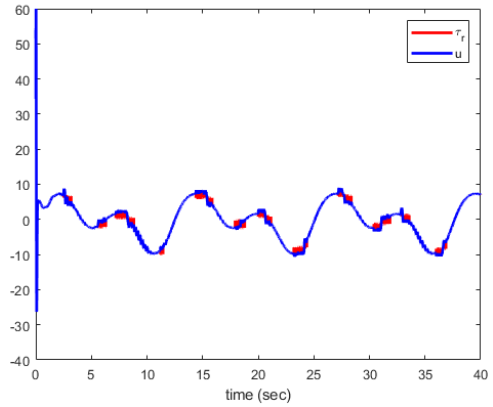

Figure 11. τ_r and u under the initial condition x_1.

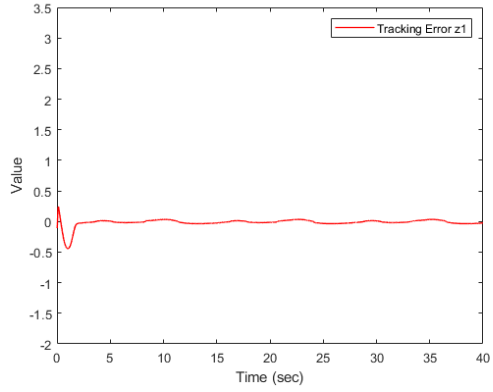

Figure 12. Error signal z_1 under the initial condition x_2.

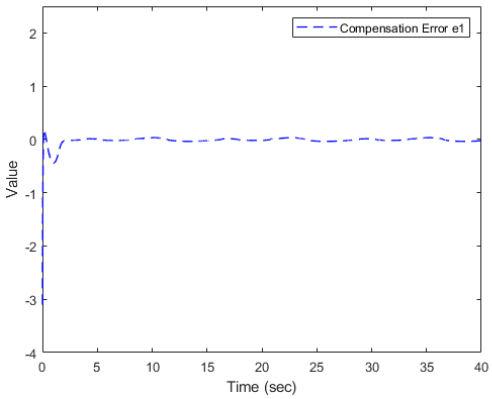

Figure 13. Filtering error e_1 under the initial condition x_2.

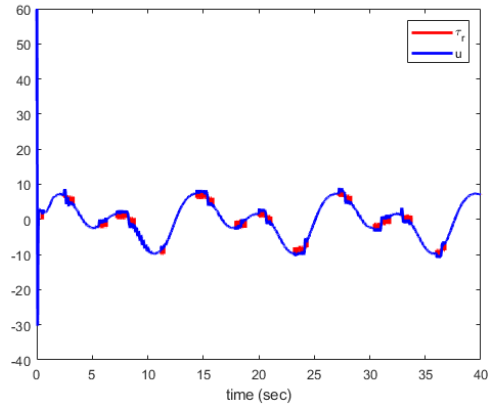

Figure 14. τ_r and u under the initial condition x_2.

4.2. Case 2

To further validate the versatility of the controller, we applied it to a variety of scenarios, demonstrating its effectiveness across different conditions and situations. The dynamic model of the aircraft exhibits strong coupling and highly nonlinear characteristics. Assuming only the motion of the aircraft in the pitch plane is considered, the longitudinal motion model of the aircraft is shown in Figure 15. The simplified longitudinal model of the aircraft can be expressed as

$$\begin{aligned}
\dot{\gamma} &= \bar{L}_\alpha \alpha - \frac{g}{V_T}\cos\gamma + \bar{L}_o \\
\dot{\alpha} &= q + \frac{g}{V_T}\cos\gamma - \bar{L}_o - \bar{L}_\alpha \alpha \\
\dot{\theta}_{\mathrm{P}} &= q \\
\dot{q} &= M_o + M_\delta \delta
\end{aligned} \tag{51}$$

where $\bar{L}_o = \frac{L_o}{mV_T}$, $\bar{L}_a = \frac{L_a}{mV_T}$, γ, α, and θ_{P} are the inclination, attack, and pitch angles of the aircraft, respectively. q is the rate of change of the pitch angle; V_T is the speed. The stable cruising speed is set to $V_T = 200$ m/s; $m = 500$ t and $g = 9.8$ m/s^2 are the aircraft mass and gravitational acceleration, respectively. L_α is the slope of the lift curve, L_o is the other influencing factors on lift, M_δ is used to control the pitching moment, M_o is the moment of another origin, usually approximated by the formula $M_o = M_a\alpha + M_q q$, and δ is the rudder declination angle, which is used as the control input. At a certain operating point, $L_o, L_\alpha, M_\alpha, M_\delta$, and M_q can be considered as unknown constants. Assuming that the speed V is stabilized within a small neighborhood of the ideal value by a linear controller (e.g., a PI controller), this can be treated as a constant. We selected $[\gamma, \alpha, q]$ as the state variables

and defined the states γ, α, and q as the control loss. Considering $u = \delta$ as the uncertainty of the model, the following triangular model in strict feedback form is obtained:

$$\begin{cases} \dot{x}_1 = p_1 x_2 + f_1(x) + d_1(t) \\ \dot{x}_2 = x_3 + f_2(x_1, x_2) + d_2(t) \\ \dot{x}_3 = p_3 u + f_3(x_2, x_3) + d_3(t) \end{cases}$$

The torque disturbance is $d_1(t) = 0.01\sin(2t)$, $d_2(t) = 0.1\cos(2t)$, $d_3(t) = 0.05\sin(t)\cos(2t)$, and $|d_i(t)| \leq \bar{d}_i$, and $\bar{d}_i > 0$. The deception attack signals suffered by the sensor network are chosen as $\kappa_1 = 1 - 3a\cos t$, $\kappa_2 = 1 - 2.3a\sin(t)$, and $\kappa_3 = 1 + 2.5a\sin(t)\cos(t)$. This random output a is still visualized in Figure 3 for clarity.

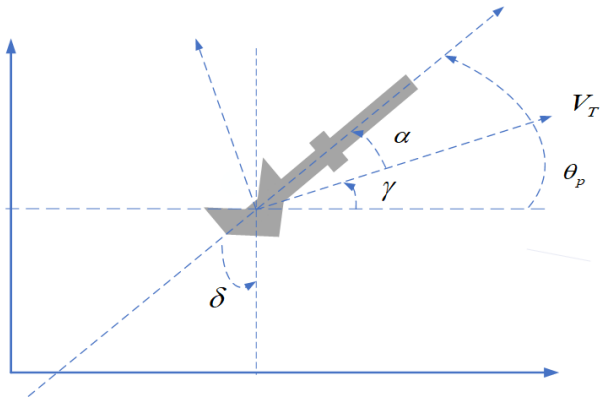

Figure 15. Schematic diagram of the aircraft longitudinal model.

In this part, we describe a simulation experiment conducted to validate the proposed control method. The controller parameters were set as follows: $m_1 = 1.1, m_2 = 1.3$, $m_3 = 1.9, \iota = \frac{2}{23}, o_1 = o_2 = o_3 = 0.01, c_1 = 15, c_2 = 1, c_3 = 0.2, \mu_1 = 4, \mu_2 = 7$, $\mu_3 = 8, \mu_{11} = 5, \mu_{21} = 8, \mu_{31} = 14$. The controller was set up to be subject to a deception attack at $T_c = 8$ s. The actuator model under deception attack is illustrated as follows:

$$u_r = \begin{cases} \alpha_3, 0 \leq t < 8 \\ (0.7 + 0.2\sin(t))\alpha_3 + x_2 x_3 + 5, t \geq 8 \end{cases} \tag{52}$$

where $\alpha_3 = -(\frac{3\Theta\pi e_3^{1+\iota}}{2T_d}\tanh(\frac{3\Theta\pi e_3^{2+\iota}}{2T_d o_3}) + \frac{3\Upsilon\pi e_3^{1-\iota}}{2T_d}\tanh(\frac{3\Upsilon\pi e_3^{2-\iota}}{2T_d o_3}) + \hat{\theta}_3||\bar{\phi}_3||\tanh(\frac{e_3||\bar{\phi}_3||}{l_3}) + c_3\vartheta_3)$, and I is a constant value of 1, which implies that the attack signal exhibits no explicit time dependency and is solely coupled with the system state via $J(x) = x_2 x_3 + 5$. In order to fully evaluate the performance of the proposed control scheme, simulations were performed using two representative initial points $x(0) = (1, 0, 1)^T$. The control objective in this subsection is to make the system output y asymptotically track the desired target trajectory $y_d = 5\sin(t)$ and to ensure that the tracking error $e(t)$ enters the preset a specified time $T_d = 2$ s. The simulation results are shown in Figures 16–19. From the above simulation results, it is clear that the proposed predefined-time control method can guarantee the system's stability within the predefined time $T_d = 2$ s and achieve good control performance. As shown in Figure 16, the system can achieve stability within the predefined time. From Figure 17, it can be inferred that, even under the influence of deception attacks, the system can still maintain good tracking performance. Figures 18 and 19, respectively, illustrate the filtering error and the control inputs.

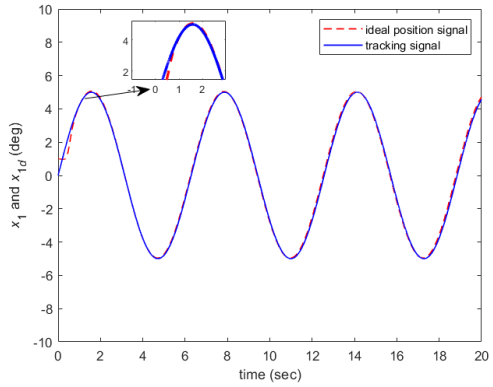

Figure 16. System output y and reference signal y_d.

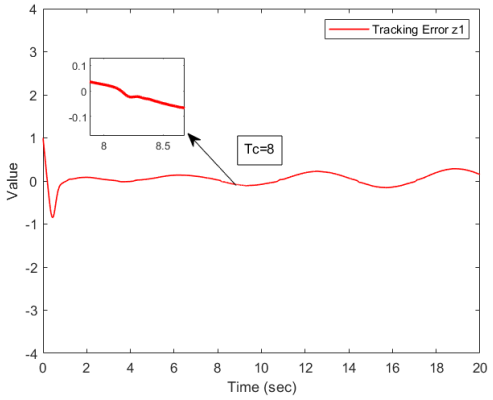

Figure 17. Error signal z_1.

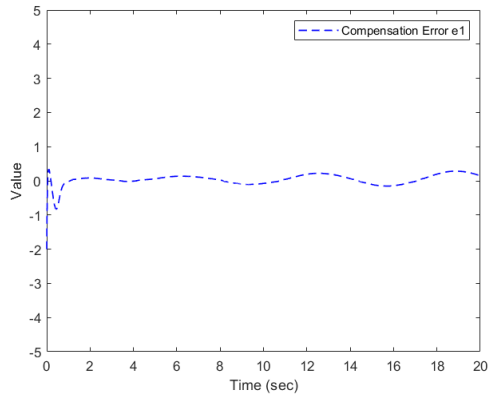

Figure 18. Filtering error e_1.

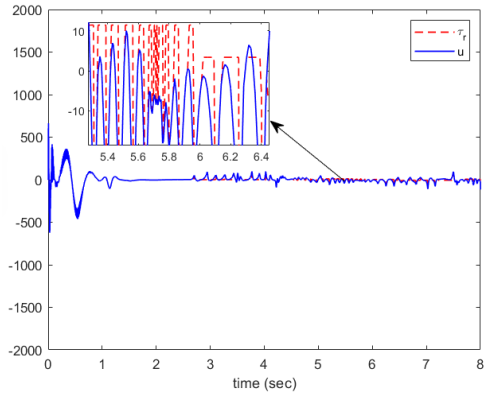

Figure 19. τ_r and u.

5. Conclusions

This study presents an innovative adaptive neural network control scheme for strict-feedback nonlinear systems vulnerable to deception attacks, with a focus on achieving precise tracking within a predefined time frame. Our approach, based on the Practical Predefined-Time Stability (PPTS) criterion, surpasses traditional methods by ensuring stability and performance within specified time bounds. To address system complexities, we integrate a novel nonlinear command filter, which enhances the handling of uncertainties and smoothness of the control input. The command filter-based predefined-time adaptive backstepping control scheme effectively counters deception attacks, a critical concern in cyber-physical systems. A key innovation is the switching threshold event-triggered mechanism, which mitigates the "complexity explosion" problem and control singularity issues, ensuring stability across various conditions. This mechanism also optimizes resource utilization by minimizing unnecessary computations and data transmissions.

Through rigorous analysis and simulations, we validate the effectiveness of our method, demonstrating predefined-time stability and strong performance under deception attacks. Additionally, we provide a comparative analysis with traditional methods, showcasing significant improvements in convergence time, robustness to deception attacks, and computational efficiency (with a 26% improvement). Future research will extend these strategies to larger systems and multi-agent applications, focusing on resilience against evolving cyber threats. We will explore scalability challenges, such as increased computational complexity and communication overhead, and develop hierarchical control frameworks and lightweight triggering mechanisms to enhance applicability in large-scale distributed cyber-physical systems, such as smart grids.

This study advances adaptive control for nonlinear systems under security threats by combining predefined-time stability, adaptive backstepping, and event-triggered mechanisms to ensure performance and security in modern control systems. Our comprehensive approach addresses key limitations of traditional methods, providing a solid foundation for future developments in the field.

Author Contributions: Methodology, J.Z.; Investigation, Z.Y.; Data curation, X.Y.; Writing—original draft, Z.Y.; Writing—review & editing, Q.Z. All authors have read and agreed to the published version of the manuscript.

Funding: This research received no external funding.

Data Availability Statement: The original contributions presented in this study are included in the article. Further inquiries can be directed to the corresponding author.

Conflicts of Interest: The authors declare no conflict of interest.

References

1. Haimo, V.T. Finite time controllers. *SIAM J. Control Optim.* **1986**, *24*, 760–770. [CrossRef]
2. Muralidharan, A.; Pedarsani, R.; Varaiya, P. Analysis of fixed-time control. *Transp. Res. Part B Methodol.* **2015**, *73*, 81–90. [CrossRef]
3. Jiménez-Rodríguez, E.; Muñoz-Vázquez, A.J.; Sánchez-Torres, J.D.; Defoort, M.; Loukianov, A.G. A Lyapunov-like characterization of predefined-time stability. *IEEE Trans. Autom. Control* **2020**, *65*, 4922–4927. [CrossRef]
4. Ren, X.X.; Yang, G.H. Adaptive control for nonlinear cyber-physical systems under false data injection attacks through sensor networks. *Int. J. Robust Nonlinear Control* **2020**, *30*, 65–79. [CrossRef]
5. Zhao, N.; Tian, Y.; Zhang, H.; Herrera-Viedma, E. Fuzzy-based adaptive event-triggered control for nonlinear cyber-physical systems against deception attacks via a single parameter learning method. *Inf. Sci.* **2024**, *657*, 119948. [CrossRef]
6. Zhu, P.; Jin, S.; Bu, X.; Hou, Z. Distributed Data-Driven Control for a Connected Autonomous Vehicle Platoon Subjected to False Data Injection Attacks. *IEEE Trans. Autom. Sci. Eng.* **2023**, *21*, 7527–7538. [CrossRef]
7. Savva, M.C. A Framework for the Detection, Localization, and Recovery from Jamming Attacks in the Internet of Things. Doctoral Thesis, University of Cyprus, Nicosia, Cyprus, 2024.

8. Verbitskiy, S.; Berikov, V.; Vyshegorodtsev, V. Eranns: Efficient residual audio neural networks for audio pattern recognition. *Pattern Recognit. Lett.* **2022**, *161*, 38–44. [CrossRef]
9. Chang, C.K.; Chang, H.H.; Boyanapalli, B.K. Application of pulse sequence partial discharge based convolutional neural network in pattern recognition for underground cable joints. *IEEE Trans. Dielectr. Electr. Insul.* **2022**, *29*, 1070–1078. [CrossRef]
10. Ciritsis, A.; Rossi, C.; Eberhard, M. Automatic classification of ultrasound breast lesions using a deep convolutional neural network mimicking human decision-making. *Eur. Radiol.* **2019**, *29*, 5458–5468. [CrossRef]
11. Sun, M.; Li, X.; Zhong, G. Semi-global fixed/predefined-time RNN models with comprehensive comparisons for time-variant neural computing. *Neural Comput. Appl.* **2023**, *35*, 1675–1693. [CrossRef]
12. Li, Y.; Zhang, W. Adaptive Neural Network Tracking Control for Nonlinear Systems with Multiple Actuator Constraints via Command Filter. *Int. J. Appl. Math. Control Eng.* **2023**, *6*, 206–214.
13. Lia, M.; Wang, L.; Meng, L.; Chang, J. Dynamic Recognition of CAPTCHA Based on Convolutional Neural Network. *Int. J. Appl. Math. Control Eng.* **2023**, *6*, 198–205.
14. Chen, W.; Zhang, Z. Globally stable adaptive backstepping fuzzy control for output-feedback systems with unknown high-frequency gain sign. *Fuzzy Sets Syst.* **2010**, *161*, 821–836. [CrossRef]
15. Chen, W.S.; Li, J.M. Globally decentralized adaptive backstepping neural network tracking control for unknown nonlinear systems. *Asian J. Control* **2010**, *12*, 96–102. [CrossRef]
16. Zheng, Y.; Sun, P.; Ren, Q.; Xu, W.; Zhu, D. A novel and efficient model pruning method for deep convolutional neural networks by evaluating the direct and indirect effects of filters. *Neurocomputing* **2024**, *569*, 127124. [CrossRef]
17. López-González, C.I.; Gascó, E.; Barrientos-Espillco, F.; Besada-Portas, E.; Pajares, G. Filter pruning for convolutional neural networks in semantic image segmentation. *Neural Netw.* **2024**, *169*, 713–732. [CrossRef]
18. Wang, Z.; Ruiz, L.; Ribeiro, A. Stability to deformations of manifold filters and manifold neural networks. *IEEE Trans. Signal Process.* **2024**, *72*, 2130–2146. [CrossRef]
19. Yin, Q.; Mu, Q.; Bian, Y.; Ji, W.; Wang, L. Command filtered dual backstepping variable structure robust switching control of uncertain nonlinear system. *Nonlinear Dyn.* **2023**, *111*, 3953–3967. [CrossRef]
20. Ma, H.; Li, H.; Lu, R.; Huang, T. Adaptive event-triggered control for a class of nonlinear systems with periodic disturbances. *Sci. China Inf. Sci.* **2020**, *63*, 150212. [CrossRef]
21. Li, B.; Xia, J.; Zhang, H.; Shen, H.; Wang, Z. Event-triggered adaptive fuzzy tracking control for stochastic nonlinear systems. *J. Frankl. Inst.* **2020**, *357*, 9505–9522. [CrossRef]
22. Vafamand, N.; Arefi, M.M.; Anvari-Moghaddam, A. Advanced kalman filter-based backstepping control of AC microgrids: A command filter approach. *IEEE Syst. J.* **2022**, *17*, 1060–1070. [CrossRef]
23. Ni, J.; Liu, L.; Tang, Y.; Liu, C. Predefined-time consensus tracking of second-order multiagent systems. *IEEE Trans. Syst. Man, Cybern. Syst.* **2019**, *51*, 2550–2560. [CrossRef]
24. Zhang, Z.; Hu, S.; Chen, Q. Predefined-Time Sliding Mode Control for Attitude Tracking of Quadrotors. *Int. J. Appl. Math. Control Eng.* **2023**, *6*, 187–191.
25. Liu, J.; Shi, J.; Wu, Y.; Wang, X.; Sun, J.; Sun, C. Event-based predefined-time second-order practical consensus with application to connected automated vehicles. *IEEE Trans. Intell. Veh.* **2023**, *8*, 4524–4535. [CrossRef]
26. Muñoz-Vázquez, A.J.; Sánchez-Torres, J.D.; Defoort, M. Second-order predefined-time sliding-mode control of fractional-order systems. *Asian J. Control* **2022**, *24*, 74–82. [CrossRef]
27. Zhang, Q.; Wang, H.; Wang, J. Finite-Time Bounded Control for Multitime-Scale Production-Inventory Systems Under Inventory Inaccuracy. *IEEE Trans. Comput. Soc. Syst.* 2024, *early access*. [CrossRef]
28. Wang, J.; Li, Y.; Wu, Y.; Liu, Z.; Chen, K.; Chen, C.P. Fixed-time formation control for uncertain nonlinear multi-agent systems with time-varying actuator failures. *IEEE Trans. Fuzzy Syst.* **2024**, *32*, 1965–1977. [CrossRef]
29. Sui, S.; Chen, C.L.P.; Tong, S. Command Filter Based Predefined Time Adaptive Control for Nonlinear Systems. *IEEE Trans. Autom. Control* **2024**, *69*, 7863–7870. [CrossRef]
30. Ji, Y.; Li, P.; Lin, Y.; Song, Y.; Gao, Q.; Liu, J. Predefined time attitude control of aircraft based on predefined time sliding mode control. *Proc. Inst. Mech. Eng. Part I J. Syst. Control Eng.* **2024**, *239*, 09596518241273990. [CrossRef]
31. Riaz, S.; Li, B.; Qi, R.; Zhang, C. An adaptive predefined time sliding mode control for uncertain nonlinear cyber-physical servo system under cyber attacks. *Sci. Rep.* **2024**, *14*, 7361. [CrossRef]
32. Zheng, W.; Qu, S.; Tang, Q. Predefined-time synchronization for uncertain hyperchaotic system with time-delay via sliding mode control. *Nonlinear Dyn.* **2024**, *112*, 21969–21987. [CrossRef]
33. Wang, S.; Wang, Y.; Li, S.; Yu, H. Predefined-time Adaptive Sliding Mode Control for Flexible Spacecraft. In Proceedings of the 2024 43rd Chinese Control Conference (CCC), Kunming, China, 28–31 July 2024; pp. 869–874.
34. Gao, Y.; Niu, B.; Chen, W.; Wang, H.; Mu, C.; Wen, G. Adaptive control of constrained nonlinear CPSs under deception attacks through sensor and actuator networks. *IEEE Trans. Circuits Syst. II Express Briefs* **2023**, *71*, 1241–1245. [CrossRef]

35. Sánchez-Torres, J.D.; Gómez-Gutiérrez, D.; López, E.; Loukianov, A.G. A class of predefined-time stable dynamical systems. *IMA J. Math. Control Inf.* **2018**, *35* (Suppl. 1), i1–i29. [CrossRef]
36. Jiménez-Rodríguez, E.; Muñoz-Vázquez, A.J.; Sánchez-Torres, J.D.; Loukianov, A.G. A note on predefined-time stability. *IFAC-PapersOnLine* **2018**, *51*, 520–525. [CrossRef]
37. Zhang, Y.; Niu, B.; Zhao, X.; Duan, P.; Wang, H.; Gao, B. Global predefined-time adaptive neural network control for disturbed pure-feedback nonlinear systems with zero tracking error. *IEEE Trans. Neural Netw. Learn. Syst.* **2021**, *34*, 6328–6338. [CrossRef]
38. Li, Z.; Yan, H.; Zhang, H.; Lam, H.K.; Wang, M. Aperiodic sampled-data-based control for interval type-2 fuzzy systems via refined adaptive event-triggered communication scheme. *IEEE Trans. Fuzzy Syst.* **2020**, *29*, 310–321. [CrossRef]
39. Yuan, X.; Chen, B.; Lin, C. Neural adaptive fixed-time control for nonlinear systems with full-state constraints. *IEEE Trans. Cybern.* **2021**, *53*, 3048–3059. [CrossRef]
40. Zuo, Z.; Tie, L. A new class of finite-time nonlinear consensus protocols for multi-agent systems. *Int. J. Control* **2014**, *87*, 363–370. [CrossRef]
41. Li, C.; Li, Y.; Zhang, J.; Li, Y. Event-Triggered Adaptive Neural Prescribed Performance Tracking Control for Nonlinear Cyber–Physical Systems against Deception Attacks. *Mathematics* **2024**, *12*, 1838. [CrossRef]

Disclaimer/Publisher's Note: The statements, opinions and data contained in all publications are solely those of the individual author(s) and contributor(s) and not of MDPI and/or the editor(s). MDPI and/or the editor(s) disclaim responsibility for any injury to people or property resulting from any ideas, methods, instructions or products referred to in the content.